bioRxiv preprint doi: https://doi.org/10.1101/850644; this version posted November 24, 2019. The copyright holder for this preprint (which was not certified by peer review) is the author/funder, who has granted bioRxiv a license to display the preprint in perpetuity. It is made available under aCC-BY-NC 4.0 International license.

1 # Evolutionary Stalling in the Optimization of
2 # the Translation Machinery

3 Sandeep Venkataram[1], Ross Monasky[2], Shohreh H Sikaroodi[1,3], Sergey
4 Kryazhimskiy[1,*,†], Betül Kaçar[2,*,†]

5 [1]Division of Biological Sciences, University of California San Diego, La Jolla, CA 92093;
6 [2]Department of Molecular and Cellular Biology, University of Arizona, Tucson, AZ 85721;
7 [3]Current address: Molecular engineering group, Fate Therapeutics Inc.
8 [*]Equal contribution
9 [†]Corresponding authors: betul@arizona.edu, skryazhi@ucsd.edu

10 ## Abstract

11 Biological organisms are modular. Theory predicts that natural selection would steadily improve
12 modules towards their performance optima up to the margin of effective neutrality. This classical
13 theory may break down for populations evolving in the clonal interference regime because
14 natural selection may focus on some modules while adaptation of others stalls. Such evolutionary
15 stalling has not been observed and it is unclear whether it limits the power of natural selection to
16 optimize module performance. To empirically characterize evolutionary stalling, we evolved
17 populations of *Escherichia coli* with genetically perturbed translation machineries (TMs). We
18 show that populations with different suboptimal TMs embark on statistically distinct trajectories
19 of TM optimization. Yet, before TMs approach the margin of effective neutrality, the focus of
20 natural selection shifts to other cellular modules, and TM optimization stalls. Our results suggest
21 that module optimization within an organism may take much longer than suggested by classical
22 theory.

23

bioRxiv preprint doi: https://doi.org/10.1101/850644; this version posted November 24, 2019. The copyright holder for this preprint (which was not certified by peer review) is the author/funder, who has granted bioRxiv a license to display the preprint in perpetuity. It is made available under aCC-BY-NC 4.0 International license.

24 # Introduction

25 Biological systems are organized hierarchically, from molecules to cells, organisms and
26 populations [1–5]. At the lowest level, molecules within cells form functional modules, such as
27 the translation machinery, or various other metabolic pathways [4,6–9]. Organismal fitness
28 depends on the performance of these modules. However, the ability of natural selection to optimize
29 cellular modules is constrained by the abundance and the effects of available beneficial mutations.

30 In the simplest case, the speed of evolutionary optimization of a module depends only on the
31 supply and the fitness effects of beneficial mutations in that module. Theoretical models predict
32 that the fitness effects of beneficial mutations will decline as the module's performance approaches
33 an optimum. Therefore, the module's performance is expected to improve steadily, albeit with a
34 gradually declining rate [10–21]. When the module's performance approaches the optimum and
35 the fitness effects of beneficial mutations drop below ~$1/N$, the inverse of the population size, the
36 optimization of the module by natural selection stops [12,22–24].

37 In reality, evolution of any one module within an organism depends on the supply and effects of
38 beneficial mutations in all modules. One reason for this interdependence is that modules are
39 encoded in genomes, and genomes are physically linked [25]. Therefore, new beneficial mutations
40 affecting different modules must compete against each other in the population whenever they
41 simultaneously arise on different genetic backgrounds [25–29]. This effect, known as "clonal
42 interference", is particularly strong when recombination is rare and the supply of adaptive
43 mutations is large [25,28], e.g., if the organism reproduces asexually, the population is large and
44 the environment is new. In the clonal interference regime, small-effect mutations are usually
45 outcompeted. Instead, adaptation is driven by mutations that provide fitness benefits above a
46 certain "clonal interference" threshold, which depends on the current supply and the fitness effects
47 of all adaptive mutations in the genome [25,29,30].

48 Beneficial mutations in different modules likely arise at different rates and have different effects
49 on the fitness of the organism. Therefore, natural selection will be "focused" on optimizing
50 modules where mutations have effects above the clonal interference threshold, while other
51 modules would adapt slowly or not at all. Modules that are more important for fitness in the current
52 environment and those that are farther from their performance optima are expected to contribute
53 more large-effect mutations. Such modules are more likely to be in the focus of natural selection.
54 However, as natural selection improves the performance of any such module, the supply and
55 effects of adaptive mutations in that module will decline. Eventually, further improvements will
56 only be possible by mutations with effects below the clonal interference threshold. At this point,
57 the evolutionary optimization of the focal module will slow down or cease entirely. We call this
58 phenomenon "evolutionary stalling".

59 Evolutionary stalling imposes a limit on the power of natural selection to improve the performance
60 of a module within an organism, in addition to the well known threshold of effective neutrality.
61 While the effective neutrality threshold cannot be overcome, evolutionary optimization of a stalled
62 module can resume once large-effect adaptive mutations in competing modules are exhausted.
63 Nevertheless, stalling poses a potentially serious obstacle for the evolutionary optimization of a
64 module because it can occur much farther from the optimum than the hard limit of effective
65 neutrality.

bioRxiv preprint doi: https://doi.org/10.1101/850644; this version posted November 24, 2019. The copyright holder for this preprint (which was not certified by peer review) is the author/funder, who has granted bioRxiv a license to display the preprint in perpetuity. It is made available under aCC-BY-NC 4.0 International license.

66 The onset of evolutionary stalling has never been directly observed. Experiments in microbes show
67 that the conditions for the onset of stalling are generally favorable. First, microbial populations
68 usually evolve in the clonal interference regime [26,31–35]. Second, when healthy strains adapt to
69 benign laboratory conditions, multiple different cellular processes are affected by beneficial
70 mutations, which suggests that multiple modules can be potentially improved by natural selection
71 [32,36–41]. On the other hand, when an important cellular module is genetically disrupted or the
72 environment is harsh, natural selection is focused on a single module [38,39,41–50]. In these cases,
73 once the poorly performing module is sufficiently improved, we expect that its further optimization
74 would eventually stall, and the focus of natural selection would shift to other modules that are still
75 suboptimal. This transition in the focus of selection has not been characterized. In particular, it
76 remains unknown how close to the performance optimum natural selection is able to push an
77 initially defective module before the onset of stalling.

78 Evolutionary stalling can be detected in two ways. If we can directly measure the performance of
79 a module over time, an abrupt reduction in the rate of its phenotypic improvement despite steady
80 increases in fitness would potentially indicate the onset of stalling. Alternatively, if we know all
81 the genes that encode a module, we could potentially infer the onset of stalling from an abrupt
82 reduction in the rate of accumulation of mutations in such genes despite continued accumulation
83 of beneficial mutations elsewhere in the genome. Both approaches are challenging because it is
84 often unclear what aspects of a module's performance are relevant for fitness and because in
85 general the location of the performance optima and the identities of all genes that encode modules
86 are unknown.

87 Here, we experimentally examine the evolution of the translation machinery (TM), one of the best
88 annotated and characterized cellular modules [8,9,51–53]. This choice allows us to use the
89 genomic approach for detecting evolutionary stalling. Extant TMs are unique in that they are close
90 to their theoretical performance optimum [54], which allows us to estimate how far from the
91 margin of effective neutrality stalling occurs. We disrupted the TM by replacing the native
92 translation Elongation Factor Tu (EF-Tu) in the bacterium *Escherichia coli* (*E. coli*) with its
93 orthologs [55–57]. We then evolved these strains in rich media where rapid and accurate
94 translation is required for fast growth [58,59]. We expect that natural selection will favor mutations
95 that repair the initial TM defects. We characterize the onset of evolutionary stalling in the TM in
96 two ways. First, we observe substitutions in known TM genes only in strains with the most severe
97 initial TM defects and quantify how far from the optimum stalling occurs. Second, we observe that
98 mutations in TM genes are exhausted within evolving populations, which provides us with direct
99 evidence for the onset of evolutionary stalling.

100

bioRxiv preprint doi: https://doi.org/10.1101/850644; this version posted November 24, 2019. The copyright holder for this preprint (which was not certified by peer review) is the author/funder, who has granted bioRxiv a license to display the preprint in perpetuity. It is made available under aCC-BY-NC 4.0 International license.

101 # Results

102 We previously replaced the native EF-Tu in *E. coli* with its orthologs from *Salmonella*
103 *typhimurium*, *Yersinia enterocolitica*, *Vibrio cholerae* and *Pseudomonas aeruginosa* and one
104 reconstructed ancestral variant [55] (Table 1). EF-Tu is encoded in *E. coli* by two paralogous
105 genes, *tufA* and *tufB*, with the majority of the EF-Tu molecules being expressed from *tufA* [60].
106 To replace all EF-Tu molecules in the cells, the *tufB* gene was deleted and the foreign orthologs
107 were integrated into the *tufA* locus [55]. We also included the control strain in which the *tufB*
108 gene was deleted and the original *E. coli tufA* was left intact. We refer to the engineered
109 "founder" *E. coli* strains as E, S, Y, V, A and P by the first letter of the origin of their *tuf* genes
110 (Table 1).

111

Strain	EF-Tu origin species	Number of amino acid differences from *E. coli* EF-Tu (percent identity)	Fitness ± SEM, % per generation
E	*Escherichia coli* (control)	0 (100)	0 ± 0.7
S	*Salmonella typhimurium*	1 (99.75)	+0.49 ± 0.09
Y	*Yersinia enterocolitica*	24 (93.91)	–3.02 ± 0.03
V	*Vibrio cholerae*	51 (87.06)	–19.0 ± 1.1
A	Reconstructed ancestor	21 (94.67)	–34.4 ± 0.7
P	*Pseudomonas aeruginosa*	62 (84.38)	–35.0 ± 0.2

112 **Table 1. Founders used for the evolution experiment.** Strains with foreign EF-Tu orthologs are ordered by their fitness
113 relative to the control E strain. SEM stands for standard error of the mean.

114 We first quantified the sub-optimality of the TMs in our founder strains. Kaçar et al. showed that
115 EF-Tu replacements lead to declines in the *E. coli* protein synthesis rate and proportional losses
116 in growth rate in the rich laboratory medium LB [55]. In our subsequent evolution experiment,
117 natural selection will favor genotypes with higher competitive fitness, which may have other
118 components in addition to growth rate [61–65]. We confirmed that EF-Tu replacements caused
119 changes in competitive fitness relative to the control E strain (Table 1), and that competitive
120 fitness and growth rate were highly correlated (Figure S1). We conclude that the competitive
121 fitness of our founders in our environment reflects their TM performance. The fitness of the S
122 and Y founders were similar to that of the control E strain (≤ 3% fitness change) indicating that
123 their TMs were at most mildly suboptimal. In contrast, the fitness of the V, A and P founders
124 were dramatically lower (≥ 19% fitness decline; Table 1) indicating that their TMs were severely
125 suboptimal.

bioRxiv preprint doi: https://doi.org/10.1101/850644; this version posted November 24, 2019. The copyright holder for this preprint (which was not certified by peer review) is the author/funder, who has granted bioRxiv a license to display the preprint in perpetuity. It is made available under aCC-BY-NC 4.0 International license.

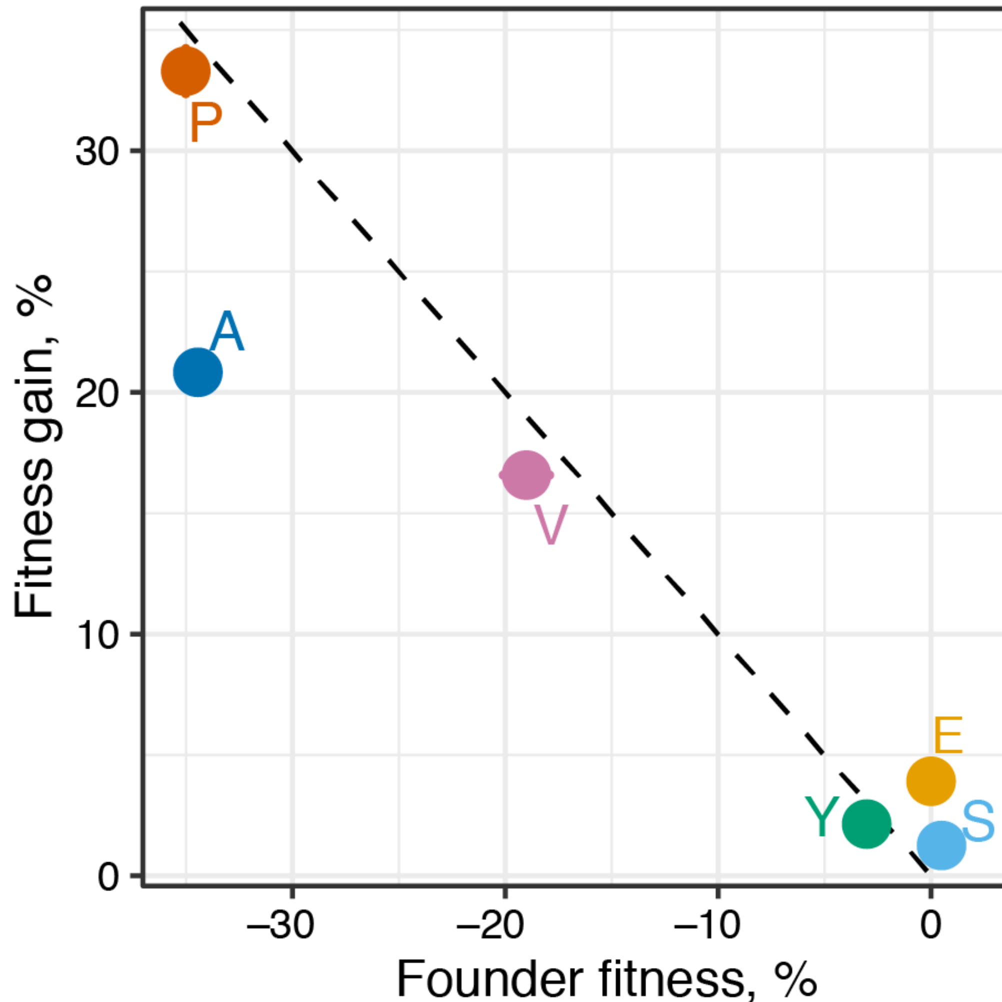

126
127 **Figure 1. Competitive fitness of founder and evolved populations.** The competitive fitness gain after
128 evolution relative to the unevolved founder averaged across replicate populations (y axis) is plotted against the
129 competitive fitness of the founder relative to the E strain (x axis). Fitness is measured in % per generation.
130 Dashed black line is $y = -x$. Populations above (below) this line are more (less) fit than the control E strain,
131 under the assumption that fitness is transitive. Error bars showing ±1 SEM are masked by the symbols (see
132 Table 1 and Figure S2).

133 Clonal interference inhibits the ability of natural selection to optimize 134 the TM

135 To determine whether natural selection focuses on restoring defective TMs, we instantiated 10
136 replicate populations from each of our six founders (60 populations total) and evolved them in
137 LB for 1,000 generations (Methods) with the bottleneck population size $N = 5\times10^5$ cells. We then
138 measured the competitive fitness of the evolved populations relative to their respective founders.
139 Fitness in all but one population increased significantly (t-test $P < 0.05$ after Benjamini-
140 Hochberg correction; Figure S2), and the average fitness increase of a population correlated
141 negatively with the initial fitness of its founder (Figure 1). These results show that even

bioRxiv preprint doi: https://doi.org/10.1101/850644; this version posted November 24, 2019. The copyright holder for this preprint (which was not certified by peer review) is the author/funder, who has granted bioRxiv a license to display the preprint in perpetuity. It is made available under aCC-BY-NC 4.0 International license.

142 substantial fitness defects caused by reductions in TM performance can be largely compensated
143 in a short bout of adaptive evolution.

144 The pattern of "declining adaptability" in Figure 1 has been frequently observed in previous
145 microbial evolution studies [37,39,41,66–70]. It could arise if adaptation is driven either by
146 mutations only in the TM, by mutations only in other modules, or by mutations in the TM and in
147 other modules. For evolutionary stalling in the TM to occur, mutations improving the TM must
148 compete against other types of mutations within the same population. To determine whether both
149 types of mutations occur in our populations, we conducted whole-population whole-genome
150 sequencing at multiple timepoints throughout the evolution experiment. This sequencing strategy
151 allows us to directly observe competition dynamics between mutations in different modules
152 [32,34,35,40].

153 We selected replicate populations 1 through 6 descended from each founder (a total of 36
154 populations), sampled each of them at 100-generation intervals (a total of 11 time points per
155 population) and sequenced the total genomic DNA extracted from these samples. We developed
156 a bioinformatics pipeline to identify de novo mutations in this data set (Methods). Then, we
157 called a mutation adaptive if it satisfied two criteria: (i) its frequency changed by more than 20%
158 in a population; and (ii) it occured in a "multi-hit" gene, i.e., a gene in which two independent
159 mutations passed the first criterion. Reliably tracking the frequencies of some types of mutations
160 (e.g., large copy-number variants) is impossible with our sequencing approach. Therefore, we
161 augmented our pipeline with the manual identification of copy-number variants which could only
162 be reliably detected after they reached high frequency in a population (Methods and Figure S3).

163 This procedure yielded 167 new putatively adaptive mutations in 28 multi-hit genes, with the
164 expected false discovery rate of 13.6%, along with an additional 11 manually-identified
165 chromosomal amplifications, all of which span the *tufA* locus (Methods and Table S1, Figure
166 S4). We classified each putatively adaptive mutation as "TM-specific" if the gene where it
167 occurred is annotated as translation-related (Methods). We classified mutations in all other genes
168 as "generic". We found that 38 out of 178 (21%) putatively adaptive mutations in 6 out of 28
169 multi-hit genes were TM-specific (Table S1). This is significantly more mutations than expected
170 by chance ($P < 10^{-4}$, randomization test) since the 215 genes annotated as translation-related
171 comprise only 4.0% of the *E. coli* genome. All of the TM-specific mutations occurred in genes
172 whose only known function is translation-related, such as *rpsF* and *rpsG*, suggesting these
173 mutations arose in response to the initial defects in the TM. The set of TM-specific mutations is
174 robust with respect to our filtering criteria (Figure S5).

175 TM-specific mutations occurred in 17 out of 36 sequenced populations. Generic mutations were
176 also observed in all of these populations (Figure S4). Thus, whenever TM-specific mutations
177 occurred, generic mutations also occurred, such that the fate of TM-specific mutations must have
178 depended on the outcome of clonal interference between mutations within and between modules
179 (Figure 2). As a result of this competition, only 14 out of 27 (52%) TM-specific mutations that
180 arose (excluding 11 *tufA* ampliciations) went to fixation, while the remaining 13 (48%)
181 succumbed to clonal interference (Figures 2, S4). In at least two of these 13 cases a TM-specific
182 mutation was outcompeted by expanding clones likely driven by generic mutations: in
183 population V6, a TM-specific mutation in *fusA* was outcompeted by a clone carrying generic
184 mutations in *fimD*, *ftsI* and *hslO* (Figure 2); in population P3, a TM-specific mutation in *tufA* was
185 outcompeted by a clone carrying generic mutations in *amiC* and *trkH* (Figure 2). We conclude
186 that, while TM-specific beneficial mutations are sufficiently common and their fitness effects are

bioRxiv preprint doi: https://doi.org/10.1101/850644; this version posted November 24, 2019. The copyright holder for this preprint (which was not certified by peer review) is the author/funder, who has granted bioRxiv a license to display the preprint in perpetuity. It is made available under aCC-BY-NC 4.0 International license.

187 at least sometimes large enough to successfully compete against generic mutations, clonal
188 interference reduces the power of natural selection to re-optimize the TM.

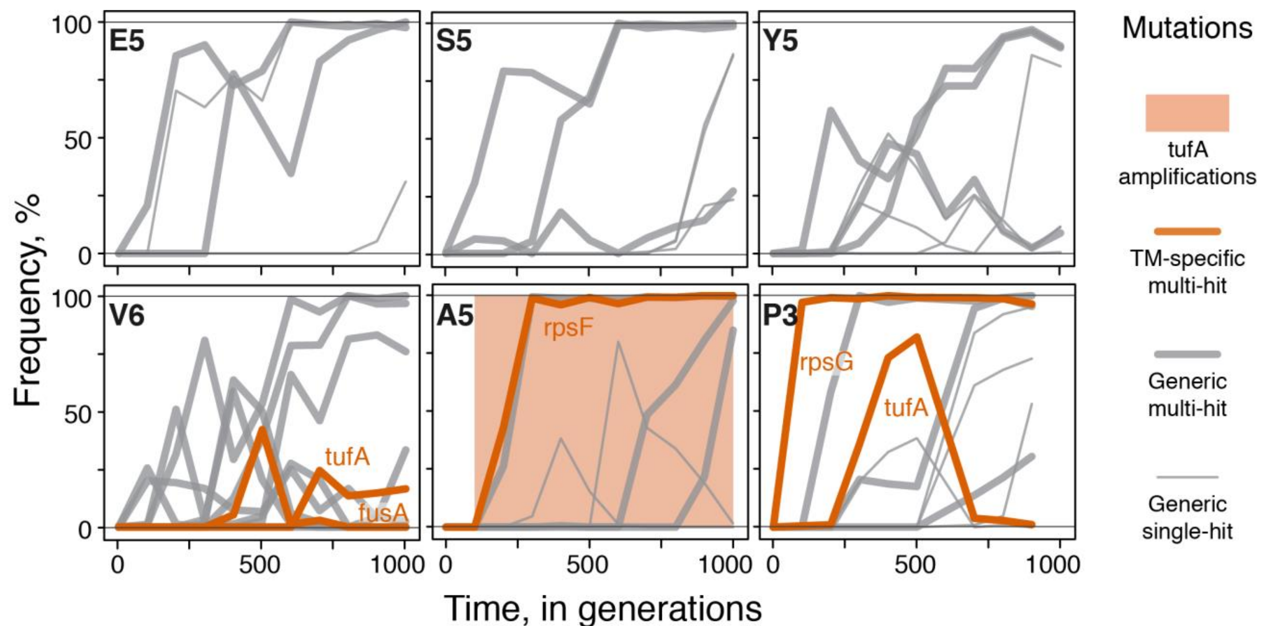

189

190 **Figure 2. Mutational trajectories in evolving populations.** Mutation frequency trajectories for one
191 representative replicate population per founder is shown (complete data for all sequenced populations can
192 be found in Figure S4). Each line represents the frequency trajectory of a single mutation. Shading
193 indicates the range of timepoints in which a *tufA* amplification was detected.

194 Evolution of the TM stalls far from the optimum

195 Competition between adaptive mutations in different modules is necessary but not sufficient for
196 evolutionary stalling to occur in any one module. Therefore, we sought direct evidence of
197 evolutionary stalling in the TM. To this end, we examined the distribution of TM-specific
198 mutations among founders and across evolutionary time. All of the detected TM-specific
199 mutations occurred in the V, A and P populations whose TMs were initially severely suboptimal;
200 no TM-specific mutations were detected in the E, S, and Y populations whose TMs were mildly
201 suboptimal (Figure 3A). Out of the 14 TM-specific mutations that eventually fixed in the V, A
202 and P populations, 12 (86%) did so in the first selective sweep (this excludes 11 *tufA*
203 amplifications). In contrast, out of the 16 generic mutations that fixed in these populations, only
204 7 (44%) did so in the first selective sweep. As a result, an average TM-specific beneficial
205 mutation reached fixation after only 300 $\pm$ 52 generations, compared to 600 $\pm$ 72 generations for
206 an average generic mutation (Figure 3B, S4). Only one (7%) TM-specific beneficial mutation
207 reached fixation after generation 600, in comparison to 9 (56%) generic beneficial mutations.
208 Thus, by the end of our evolution experiment, adaptive TM-specific mutations are depleted even
209 in populations descended from the V, A and P founders.

bioRxiv preprint doi: https://doi.org/10.1101/850644; this version posted November 24, 2019. The copyright holder for this preprint (which was not certified by peer review) is the author/funder, who has granted bioRxiv a license to display the preprint in perpetuity. It is made available under aCC-BY-NC 4.0 International license.

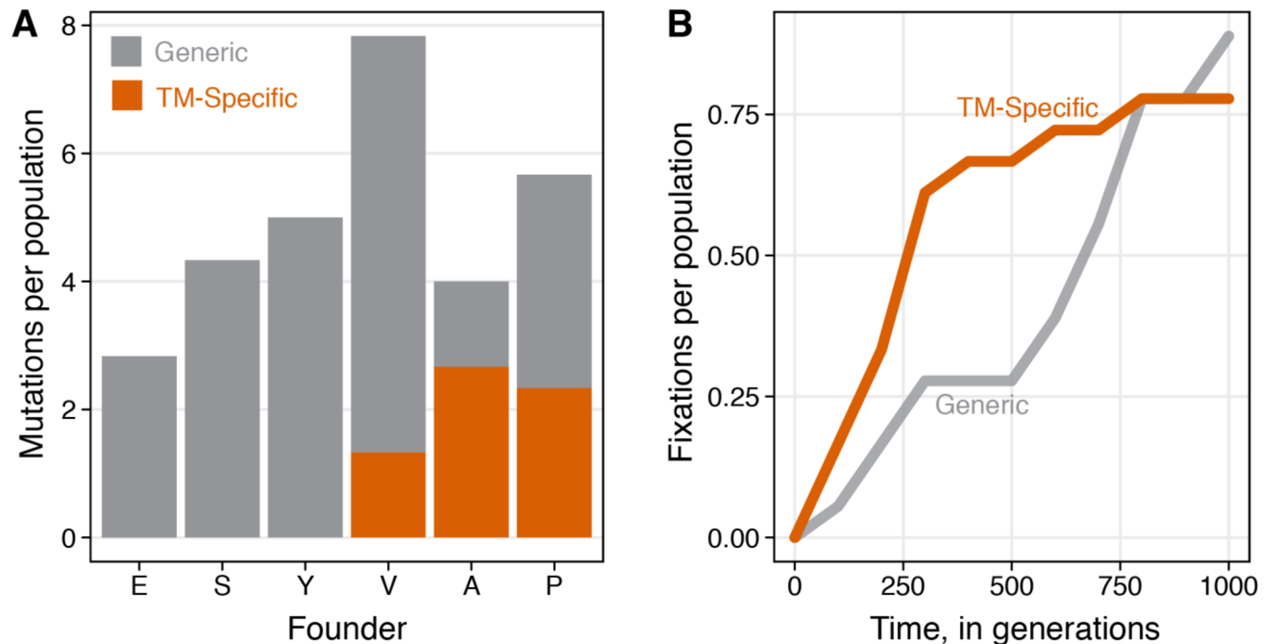

210

211 **Figure 3. Evidence for stalling in the evolutionary optimization of the TM. A.** Number of adaptive
212 TM-specific and generic mutations identified in the six sequenced populations derived from each of the
213 founders. **B.** Cumulative number of fixed TM-specific or generic mutations per population derived
214 from the V, A and P founders.

215 These data demonstrate that evolutionary stalling in the optimization of the TM occurs in our
216 populations. They also allow us to place bounds on the TM defects which can and cannot be
217 improved by natural selection prior to the onset of evolutionary stalling. First, consider the
218 founder Y in which the initial defect in the TM incurs a ~3% fitness cost (Table 1). While Y
219 populations gained on average 2.4% in fitness during evolution (Figure 1), none of these gains
220 are attributed to TM-specific mutations. This indicates that TM adaptation is stalled if the initial
221 TM defect incurs $\leq 3\%$ fitness cost. Next, consider founder V in which the initial defect in the
222 TM incurs a ~19% fitness cost (Table 1). We observed 8 TM-specific mutations across all V
223 populations, including three *tufA* amplifications. At least one of these mutations reached fixation
224 (Figure S4), suggesting that natural selection can repair defects in the TM that incur $\geq 19\%$
225 fitness cost without the onset of evolutionary stalling. We conclude that the focus of natural
226 selection shifts from optimizing the TM to other cellular modules when the TM incurs a fitness
227 cost somewhere between 3% and 19%.

228 Another way of arriving at a lower bound for the onset of stalling is to consider the V, A and P
229 populations. On average, these populations fixed 0.8 TM-specific mutations during evolution,
230 and remained ~5.3% less fit than the control E strain, assuming fitness is transitive (Figure 1).
231 Even if we conservatively attribute all these fitness gains to improvements in the TM, by the end
232 of the experiment, TMs in these populations must still be on average ~5.3% below the optimum.
233 Yet, by the end of the experiment, fixation of TM mutations had essentially stopped, while
234 fixation of generic mutations continued unabated (Figures 3B). This suggests that TMs that incur
235 fitness defects larger than 3% may still be subject to evolutionary stalling.

236 To further corroborate and possibly refine these bounds, we selected two TM-specific mutations
237 that arose in our populations, genetically reconstructed them in their respective founder strains
238 and directly measured their fitness benefits. The TM-specific mutation A74G in the *rpsF* gene,

bioRxiv preprint doi: https://doi.org/10.1101/850644; this version posted November 24, 2019. The copyright holder for this preprint (which was not certified by peer review) is the author/funder, who has granted bioRxiv a license to display the preprint in perpetuity. It is made available under aCC-BY-NC 4.0 International license.

239 which arose in population A5, provides an 8.2 ± 1.0% fitness benefit in the A founder. The TM-
240 specific mutation G331A in gene *rpsG*, which arose in populations P2, P3 and P5, provides a 6.5
241 ± 1.2% fitness benefit in the P founder. Such large-effect mutations can never arise in TMs that
242 incur a less than 6.5% fitness cost, which is further indirect evidence that TM adaptation stalls
243 when it incurs a fitness cost larger than our conservative 3% bound.

244 If the TM was the only suboptimal module in the cell, theory suggests that its adaptation would
245 continue until the fitness defect it incurs is $\frac{n-1}{8N}$, where n is the effective number of TM
246 phenotypes relevant for fitness and N is the population size [12]. Although n is unknown, it is
247 typically thought to be small, even for entire organisms [18,71]. Assuming that $n \lesssim 10^3$, which
248 seems reasonable given that there are roughly 215 translation-related genes in *E. coli* (Methods),
249 the effective neutrality threshold is $\lesssim 0.025\%$. As the TM is not the only module that natural
250 selection needs to optimize, its adaptation stalls orders of magnitude above the theoretically
251 predicted effective neutrality threshold.

252 Epistasis and historical contingency in TM evolution

253 We observed that natural selection improved all severely suboptimal TMs, but it is unclear
254 whether different TM defects can be alleviated by a common set of mutations or whether
255 repairing each TM defect requires its own unique solution. Previous work has shown that genetic
256 interactions (or "epistasis") between mutations in the TM have been important in the
257 evolutionary divergence of TMs along the tree of life [55,72–75]. We reasoned that genetic
258 interactions might be similarly important in the short bout of evolution observed in our
259 experiment. Specifically, we asked whether different initial TM variants acquired adaptive
260 mutations in the same or in different translation-associated genes.

261 We found that 4 out of 7 classes of TM-specific mutations arose in a single founder (Figure 4A).
262 For example, we detected six independent mutations in the *rpsG* gene, which encodes the
263 ribosomal protein S7, and all of these mutations occurred in the P founder ($P < 10^{-4}$,
264 randomization test with Benjamini-Hochberg correction, Methods). Similarly, all four mutations
265 in the *rpsF* gene, which encodes the ribosomal protein S6, occurred in the A founder ($P < 10^{-4}$,
266 randomization test with Benjamini-Hochberg correction). To directly measure how the effects of
267 these mutations vary across genetic backgrounds, we attempted to genetically reconstruct
268 mutation A74G in the *rpsF* gene and mutation G331A in *rpsG* gene in all six of our founder
269 strains. We successfully reconstructed both of these mutations in the founder strains in which
270 they arose and confirmed that they were strongly beneficial, as described above (8.2 ± 1.0% and
271 6.5 ± 1.2% benefit, respectively). In contrast, our multiple reconstruction attempts in all other
272 founders were unsuccessful (Methods), suggesting that these mutations are strongly deleterious
273 in all other genetic backgrounds that we tested.

274 These results suggest that genetic interactions between different TM components cause initially
275 different TM variants to embark on divergent adaptive trajectories and lead to historical
276 contingency and entrenchment in TM evolution [76–78].

bioRxiv preprint doi: https://doi.org/10.1101/850644; this version posted November 24, 2019. The copyright holder for this preprint (which was not certified by peer review) is the author/funder, who has granted bioRxiv a license to display the preprint in perpetuity. It is made available under aCC-BY-NC 4.0 International license.

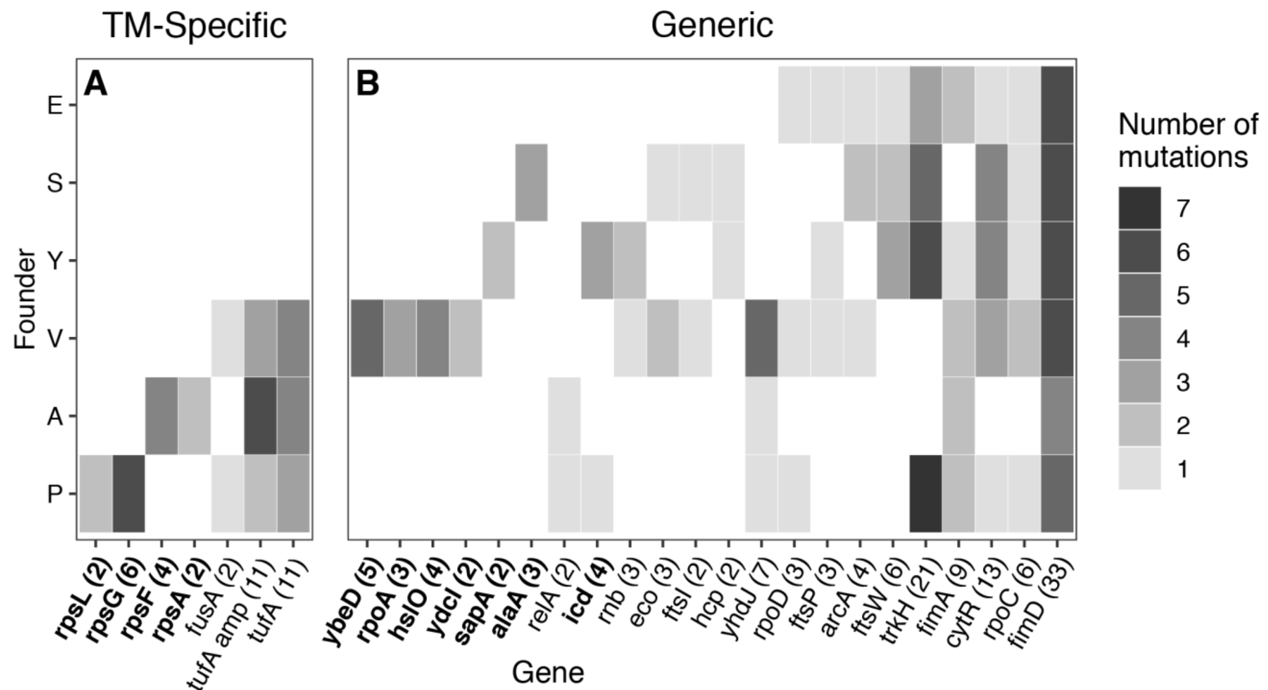

277

278 **Figure 4. Distribution of putatively adaptive mutations.** Heatmap of all putatively adaptive mutations
279 identified via whole-genome sequencing, grouped by founder and by gene. Amplification of the *tufA*
280 locus are counted separately from other mutations in *tufA*. **A.** Translation-associated genes **B.** All other
281 genes. Genes in bold are those where mutations were detected in significantly fewer founders than
282 expected by chance ($P < 0.05$, Benjamini-Hochberg correction, see Methods). Numbers in parentheses
283 indicate the total number of mutations in that gene observed across all sequenced populations.

284 Genome-wide adaptive responses to TM perturbations

285 Adaptive evolution of the TM stalls because natural selection acts on multiple cellular modules
286 in *E. coli*, all of which are encoded on a single non-recombining chromosome. However,
287 modules are linked not only physically by the encoding DNA but also functionally in that they
288 all contribute to the fitness of the organism. This functional interdependence implies that
289 mutations in one module may alter the selection pressure on other modules. For example,
290 improvements in translation efficiency may increase the selection pressure to improve efficiency
291 of catabolic reactions, analogously to the "shifting and swaying of selection coefficients" on
292 enzymes in the same metabolic pathway discussed in the classic work by Hartl et al. [22].
293 Therefore, in addition to intra-module epistasis demonstrated above we might expect inter-
294 module epistasis, such that initially different TM variants could precipitate distinct adaptive
295 responses in the rest of the genome. To test this hypothesis, we examined the distribution of
296 generic mutations among founder genotypes.

297 We found that generic mutations in 7 out of 22 genes occurred in fewer founders than expected
298 by chance (Figure 4B, Methods). For example, we detected five independent mutations in the
299 *ybeD* gene, which encodes a protein with an unknown function, and all these mutations occurred
300 in the V founder ($P < 10^{-4}$, randomization test with Benjamini-Hochberg correction). Similarly,
301 all three mutations in the *alaA* gene, which encodes a glutamate-pyruvate aminotransferase,
302 occurred in the A founder ($P < 10^{-4}$, randomization test with Benjamini-Hochberg correction).
303 To corroborate these statistical observations, we reconstructed the T93G mutation in the *ybeD*

bioRxiv preprint doi: https://doi.org/10.1101/850644; this version posted November 24, 2019. The copyright holder for this preprint (which was not certified by peer review) is the author/funder, who has granted bioRxiv a license to display the preprint in perpetuity. It is made available under aCC-BY-NC 4.0 International license.

304 gene in all six founder strains and directly measured its fitness effects. As expected, this
305 mutation confers a 5.9% fitness benefit in the V founder. In contrast, it is strongly deleterious in
306 the P founder and indistinguishable from neutral in the remaining founders (Figure 5). These
307 results show that at least some genetic perturbations in the TM can have genome-wide
308 repercussions. They can precipitate bouts of genome-wide adaptive evolution that are contingent
309 on the initial perturbations in the TM.

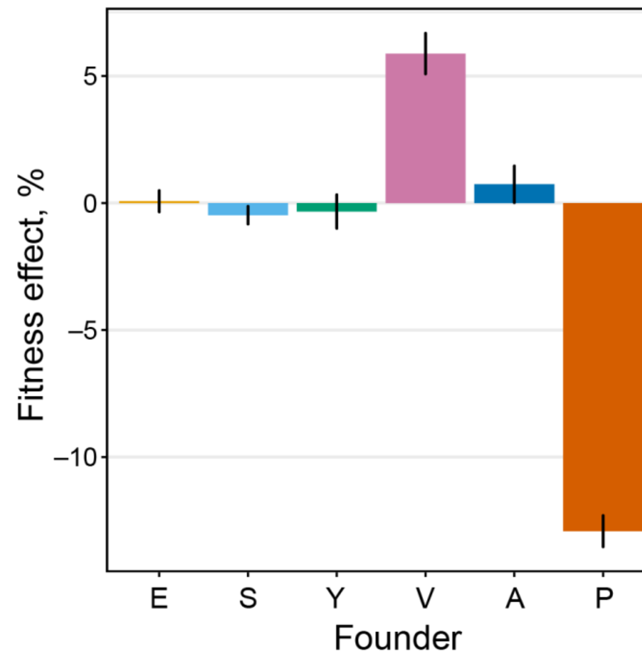

310

311 **Figure 5. Fitness effect of the *ybeD* T193D mutation in different founders.** Fitness effect of the
312 mutation is measured in a direct competition of each founder with the mutation against the founder without
313 the mutation. Error bars show the SEM.

314

bioRxiv preprint doi: https://doi.org/10.1101/850644; this version posted November 24, 2019. The copyright holder for this preprint (which was not certified by peer review) is the author/funder, who has granted bioRxiv a license to display the preprint in perpetuity. It is made available under aCC-BY-NC 4.0 International license.

315 # Discussion

316 The fitness of an organism depends on the performance of many molecular modules inside cells.
317 While natural selection favors genotypes with better-performing modules, it is difficult for
318 evolution to optimize multiple modules simultaneously, particularly when recombination rates
319 are low and many adaptive mutations in different modules are available. In this regime, natural
320 selection is expected to focus on optimizing those modules where many mutations provide large
321 fitness benefits, while the adaptive evolution in other modules stalls. Here we have documented
322 and characterized the evolutionary stalling of the translation machinery (TM) in *E. coli*.

323 We found that evolutionary optimization of the TM was slowed down by competition with
324 adaptive mutations in the rest of the genome (Figure 2). The populations whose TMs were
325 initially mildly sub-optimal (incurring $\lesssim 3\%$ fitness cost) adapted by acquiring mutations that did
326 not directly affect the TM. In contrast, populations whose TMs were initially severely sub-
327 optimal (incurring $\gtrsim 19\%$ fitness cost) rapidly discovered and fixed TM-specific beneficial
328 mutations. We conclude that the adaptive evolution of the TM stalls when the TM defect incurs a
329 fitness cost between 3% and 19%. This is a conservative lower bound on the onset of stalling that
330 we derived under the assumption that the TM in the control E strain is close to optimal.
331 However, the E strain itself suffers a $4.1 \pm 0.1\%$ fitness defect relative to wild-type *E. coli* that
332 contains the *tufB* gene (Methods). Thus, the adaptive evolution of the TM may actually stall
333 when the TM defect incurs a fitness cost between 7.1% and 23.1%.

334 Evolutionary stalling in the TM occurs for one of two reasons. First, the rate of TM-specific
335 beneficial mutations may be too low for these mutations to survive genetic drift when rare.
336 Alternatively, these mutations occur frequently enough to survive drift but succumb to clonal
337 interference. Both theoretical and empirical (albeit limited) evidence suggest that small-effect
338 beneficial mutations are more common than large-effect mutations [16,19,79,80]. The fact that
339 we observed TM-specific mutations with effects $\geq 5\%$ indicates that the rate of such mutations is
340 high. We expect the rate of TM-specific mutations with effects $< 5\%$ to be even higher. If we
341 relax the stringency criteria for detecting beneficial mutations, we find one TM-specific mutation
342 in the gene *rbbA* in the population E5 (Figure S5). This suggests that small-effect TM-specific
343 beneficial mutations exist and supports the conjecture that adaptation of the TM stalls because of
344 clonal interference.

345 Our results show that evolutionary stalling limits the ability of natural selection to improve a
346 module, but this limit is not absolute. As a population accumulates beneficial mutations in other
347 modules, their supply will be depleted and their fitness effects will likely decrease due to
348 diminishing returns epistasis [37,66,67,81–83]. These changes will in turn increase the chances
349 for small-effect mutations in the focal module to survive clonal interference thereby overcoming
350 evolutionary stalling. While we did not observe resumption of adaptive evolution in the TM in
351 this experiment, we find some evidence for such a transition in one other module. We detected
352 11 mutations in multi-hit genes that affect cytokinesis (Methods, Figures S6, S7). Most of these
353 mutations reached high frequency in the second half of the experiment, suggesting that
354 adaptation in the cytokinesis module was initially stalled and then resumed.

bioRxiv preprint doi: https://doi.org/10.1101/850644; this version posted November 24, 2019. The copyright holder for this preprint (which was not certified by peer review) is the author/funder, who has granted bioRxiv a license to display the preprint in perpetuity. It is made available under aCC-BY-NC 4.0 International license.

355 ## General implications for the evolution of modular systems

356 Evolutionary stalling can occur much farther from the optimum than the margin of effective
357 neutrality, which poses a potentially serious obstacle for evolutionary optimization, in particular
358 when selection pressures vary over time. To overcome evolutionary stalling in a module, the
359 supply of large-effect beneficial mutations in other modules must be depleted. However,
360 variability in selection pressures can replenish this supply, leaving the focal module stalled far
361 from the optimum. Thus, long periods of time under constant selection pressures might be
362 required for natural selection to fully optimize even essential modules.

363 Our results imply that it is impossible to fully understand the evolution a cellular module in
364 isolation from the genome where it is encoded and the population-level processes that govern
365 evolution. The ability of natural selection to optimize any one module depends on the population
366 size, the rate of recombination, the supply and the fitness effects of all beneficial mutations in the
367 genome and on how these quantities change as the population adapts. Further theoretical work
368 and empirical measurements integrated across multiple levels of biological organization are
369 required for us to understand adaptive evolution of modular biological systems.

370 ## Implications for the evolution the translation machinery

371 In this work, we identified several TM-specific adaptive mutations, but their biochemical and
372 physiological effects are at this point unknown. However, the fact that 11 chromosomal
373 amplifications and 12 noncoding or synonymous events occurred in the *tufA* operon suggests that
374 some of the TM-specific mutations are beneficial because they adjust EF-Tu abundance in the
375 cell. This would be consistent with previous evolution experiments [46,84,85]. Directly
376 measuring the phenotypic effects of the TM-specific mutations described here is an important
377 avenue for future work.

378 Our results give us a glimpse of the fitness landscape of the TM. This landscape is broadly
379 consistent with Fisher's geometric model in that the distribution of fitness effects of beneficial
380 mutations depends on the distance to the performance optimum [10,16,21]. However, Fisher's
381 model does not inform us how many distinct genotypes encode this optimum and how they are
382 connected in the genotype space. We observed that evolutionary trajectories originating at
383 different initial defective TMs gained distinct TM-specific adaptive mutations. This suggests that
384 the TM performance optimum is encoded by multiple genotypes that either form a single
385 contiguous neutral network [86] or multiple isolated neutral networks [87]. Moreover, we
386 observed that most of our populations with initially severely suboptimal TMs were able to
387 discover TM-specific mutations. This suggests that genotypes that encode high-performing TMs
388 may be present in the mutational neighborhoods of many genotypes [86,88].

389 How did the translation machinery historically evolve on this fitness landscape? Extant TMs are
390 thought to be nearly optimal [54], but when and how TMs evolved to this optimal state is
391 unknown. Our work helps us constrain the plausible evolutionary scenarios. One possibility is
392 that the TM approached the optimum prior to the last universal common ancestor (LUCA), and
393 subsequent evolution in TM components along most lineages was driven by conditionally neutral
394 and mildly deleterious substitutions. Another possibility is that the TM in LUCA was not
395 optimal, and TMs in different lineages were optimized after LUCA. Our results suggest that
396 evolving an optimal TM after it was encapsulated in a cell with a physically contiguous genome

bioRxiv preprint doi: https://doi.org/10.1101/850644; this version posted November 24, 2019. The copyright holder for this preprint (which was not certified by peer review) is the author/funder, who has granted bioRxiv a license to display the preprint in perpetuity. It is made available under aCC-BY-NC 4.0 International license.

397 may have been difficult, especially if other components of the cell also required continuous
398 adaptation to a changing environment. In other words, the possibility that the TM has been
399 functionally optimized prior to LUCA appears more likely.

400

bioRxiv preprint doi: https://doi.org/10.1101/850644; this version posted November 24, 2019. The copyright holder for this preprint (which was not certified by peer review) is the author/funder, who has granted bioRxiv a license to display the preprint in perpetuity. It is made available under aCC-BY-NC 4.0 International license.

401 # Materials and methods

402 ## Materials, data and code availability

403 All strains and plasmids constructed and used in this work are available per request. Raw
404 sequencing data were analyzed with the python-based workflow implemented in Ref. [40] and
405 run on the UCSD TSCC computing cluster via a custom python wrapper script. All analysis and
406 plots reported in this manuscript have been performed using the R computing environment. The
407 script, modified reference genomes and the raw data (except for raw sequencing data) used for
408 analysis can be found at https://github.com/sandeepvenkataram/EvoStalling. Raw sequencing
409 data for this project have been deposited into the NCBI SRA under project PRJNA560969.

410 ## Media and culturing conditions

411 Liquid medium is the Luria-Bertani medium (LB) (per liter, 10 g NaCl, 5 g yeast extract, and 10
412 g tryptone) and solid medium is LBA (LB with 1.5% agar), unless noted otherwise. All
413 incubations were done at 37°C, and liquid cultures were shaken at 200 rpm for aeration, unless
414 noted otherwise. All media components and chemicals were purchased from Sigma, unless noted
415 otherwise.

416 ## Strains and plasmids

417 All strains in this study were derived from *E. coli* K12 MG1655. Strain genotypes are listed in
418 Table S2. Complete methods for the construction of the E, S, Y, V, A and P strains, which harbor
419 a single *tuf* gene variant replacing *tufA* gene, can be found in Ref. [55]. Strains with engineered
420 *ybeD*, *rpsF* and *rpsG* mutations were constructed using the same method, except the
421 chromosomal *kanR* marker was not removed (Figure S9). For a full list of primer sequences used
422 for *ybeD*, *rpsF* and *rpsG* engineering, see Table S2.

423 Plasmids pZS1-TnSL and pZS2-TnSL were used in competition assays to provide Ampicillin
424 and Kanamycin resistance, respectively. pZS1-TnSL, derived from pUA66 [89], was kindly
425 provided by Georg Rieckh. pZS2-TnSL was constructed from pZS1-TnSL by replacing the
426 *ampR* cassette with *kanR*.

427 ## Evolution experiment

428 Experimental evolution was performed by serial dilution at 37°C in LB broth. To start the
429 evolution experiment, an initial 5 mL overnight culture was inoculated from a single colony from
430 the frozen stock of each founder strains. 10 replicate populations were started from single
431 colonies derived from these overnight cultures. The replicates were serially transferred every 24h
432 (±1h) as follows: 100 µL of saturated culture were transferred into 10 mL saline solution (145
433 mM NaCl), 50 µL of these dilutions were then transferred to 5 mL fresh LB (tubes were
434 vigorously vortexed prior to pipetting). This resulted in a bottleneck population size of about
435 5×10^5 cells. Freezer stocks (200 µL of 20% glycerol + 1 mL saturated culture) were prepared
436 approximately every 100 generations and stored at –80°C.

bioRxiv preprint doi: https://doi.org/10.1101/850644; this version posted November 24, 2019. The copyright holder for this preprint (which was not certified by peer review) is the author/funder, who has granted bioRxiv a license to display the preprint in perpetuity. It is made available under aCC-BY-NC 4.0 International license.

437 ## Competitive fitness assays

438 To carry out pairwise competition assays, an Ampicillin-resistant and a Kanamycin-resistant
439 versions of the query and reference strains/populations were generated by transforming these
440 strains/populations with plasmids pZS1-TnSL and pZS2-TnSL, using standard methods [90].
441 Two replicate competition assays were performed for each query-reference pair with reciprocal
442 markers (four assays total per pair), except for allele-replacement mutants (see below). To
443 validate that the resistance-marker plasmids do not differentially impact fitness in any of the six
444 founder genetic backgrounds, we carried out three-way competition assays between the KanR-
445 marked, AmpR-marked and the unmarked versions of the founders (Figure S8). Since the allele-
446 replacement mutants carry a chromosomal *kanR* marker (see above), they were only competed
447 against AmpR reference strains.

448 To start a competition assay, a query and a reference cultures were scraped from frozen stocks
449 and inoculated into 5 mL LB-Amp or LB-Kan media as appropriate. After about 24 hours, the
450 query and the reference cultures were mixed together in ratio 1:9 and diluted 1:10,000 into 5 mL
451 fresh LB media. After that, the mixed culture was propagated as in the evolution experiment. To
452 determine the relative abundances of the query and reference individuals in the mixed culture,
453 100 µl of appropriately diluted cultures were plated on both LB-Amp and LB-Kan plates after
454 24, 48 and 74 hours of competition. For some competitions, where fitness differences were
455 particularly large or small, samples from 0 or 96 hours were also obtained. Plates were
456 photographed after an ~24-hour incubation period (when colonies were easily visible) and
457 colonies were automatically counted with the OpenCFU software [91]. In each competition, we
458 estimated the fitness of the query strain relative to the reference strain by linear regression of the
459 natural logarithm of the ratio of the query to reference strain dilution-adjusted colony counts
460 against time. Variance was also estimated from these regressions. Replicate measurements were
461 combined into the final estimate using the inverse variance weighting method.

462 Competitions between two reciprocally marked versions of the same strain represent a special
463 case. If the two marker-carrying plasmids impose exactly the same fitness cost, our competition
464 assay between two reciprocally marked versions of the same strain is fully symmetric, which
465 implies that in expectation it must yield a fitness value of exactly zero. Any estimate of fitness
466 from a finite number of measurements even in such idealized fully symmetric case will not zero.
467 However, such deviations from zero would reflect only measurement noise rather than any
468 biologically meaningful fitness difference. In reality, the two marker-carrying plasmids may
469 impose slightly different fitness costs, but because the difference in the cost is detectable (see
470 above), we still interpret deviations from zero in our fitness estimates as noise. Therefore, in
471 competitions of reciprocally marked versions of the same strain, we set our fitness estimate to
472 zero and use the four fitness values obtained from the replicate assays to estimate the noise
473 variance as the average of the squared fitness value.

474 ## Growth rate assays

475 Strains were inoculated from frozen stock into 5 mL LB media in 15 mL culture tubes and grown
476 overnight. After 24 hours of growth, the cultures were diluted 1:100 into fresh 5 mL of media
477 and grown for 4 hours. They were diluted again 1:100 into 200 µl of LB in flat-bottom Costar 96
478 well microplates (VWR Catalog #25381-056) and grown in a Molecular Devices SpectraMax i3x

bioRxiv preprint doi: https://doi.org/10.1101/850644; this version posted November 24, 2019. The copyright holder for this preprint (which was not certified by peer review) is the author/funder, who has granted bioRxiv a license to display the preprint in perpetuity. It is made available under aCC-BY-NC 4.0 International license.

479 Multi-mode microplate reader at 37°C with shaking for 24 hours with absorbance measurements
480 at 600 nm every 15 minutes. Three replicate growth measurements were conducted for each
481 strain. Optical density data were first ln-transformed. A linear regression model was fit to all sets
482 of 5 consecutive data points where OD was below 0.1. Growth rate for the culture was estimated
483 as the maximal slope across all of these 5-point regressions. The mean growth rate and standard
484 error of the mean were calculated from replicate measurements.

485 Genome sequencing

486 Whole-genome sequencing was conducted for population samples of 6 replicate populations for
487 each of the 6 founders (36 total populations). Each population was sequenced at 11 timepoints,
488 every 100 generations beginning at generation 0. Four lanes of 100 bp paired end sequencing
489 was conducted at the UCSD IGM Genomics center on an Illumina HiSeq 4000 machine. The
490 average per-base-pair coverage across all samples was 131x. Samples E1_t600, E2_t500,
491 Y3_t600, P3_t600, P2_t800, P2_t1000 and A1_t700 yielded data inconsistent with the rest of the
492 allele frequency trajectories from the same population, likely due to mislabelling during sample
493 preparation. These samples were subsequently removed from our analysis.

494 DNA extraction and library preparation

495 To minimize competitive growth during handling, 100 µl of a 1:10,000 dilution of frozen stock
496 from each sample was plated on LB agar plates and incubated at 37°C overnight. The entire plate
497 of colonies was then scraped and used for genomic DNA extraction. DNA extractions were
498 conducted using the Geneaid Presto mini gDNA Bacteria Kit (#GBB300) following the
499 manufacturer's protocol. Library preparation was conducted using a modified Illumina Nextera
500 protocol as described in [92].

501 Validation of variants with Sanger sequencing

502 43/45 variants, particularly those in loci previously annotated to be involved with translation,
503 were validated using Sanger sequencing. Briefly, populations and timepoints containing the
504 variant at substantial frequency were identified, and clones isolated for genomic DNA extraction,
505 PCR and Sanger Sequencing using standard protocols. The primers used for this validation are
506 detailed in Table S3. The two mutations that failed to validate were expected to be at relatively
507 low frequency in their populations (17% and 38%), so additional clone sampling may be
508 required to validate these events.

509 Analysis of sequencing data

510 Variant calling

511 Sequenced samples were mapped to the MG1655 reference genome (NCBI accession U00096.3)
512 and variants were called using a custom breseq-based pipeline described in Supplementary text
513 section 4 of Ref. [40] and kindly provided to us by Dr. Benjamin Good. Briefly, this method
514 leverages the fact that each population was sampled multiple times across the evolution

bioRxiv preprint doi: https://doi.org/10.1101/850644; this version posted November 24, 2019. The copyright holder for this preprint (which was not certified by peer review) is the author/funder, who has granted bioRxiv a license to display the preprint in perpetuity. It is made available under aCC-BY-NC 4.0 International license.

515 experiment to increase our ability to distinguish real low-frequency variants from sequencing
516 errors and other sources of noise.

517 The reference genome was modified with the appropriate *tufA* sequence for each genetic
518 background used in the evolution experiment along with the removal of the *tufB* sequence, and
519 annotation coordinates were lifted over to be consistent with the original MG1655 reference
520 sequence using custom scripts. The modified reference genomes and annotation files are
521 included in the github repository. The variants reported in Table S1 have been lifted back to be
522 compatible with the original MG1655 reference genome.

523 Annotation

524 Variant annotation was conducted using the software package ANNOVAR[93]. Coding variants
525 were established as normal, while noncoding variants were annotated as being associated with
526 the closest gene (in either strand, in either direction) in the genome, as long as it was less than 1
527 kb away. As ANNOVAR is not set up to work with *E. coli* by default, the *E. coli* MG1655
528 nucleotide annotation was downloaded in GFF3 form from NCBI Genbank (U00096.3).
529 Cufflinks[94] gffread tool was used to convert this file to GTF, which was then converted to
530 GenePred by using the UCSC Genome Browser gtfToGenePred tool. The final annotation file
531 was generated using the ANNOVAR retrieve_seq_from_fasta.pl script. The annotation file was
532 lifted over to be compatible with each reference sequence.

533 Copy number variants were called manually using genome-wide coverage plots generated using
534 samtools[95] "view" command and the R computing environment. As these variants have their
535 frequency confounded with their copy number, only their presence/absence was noted for
536 downstream analysis.

537 Filtering

538 We considered single nucleotide polymorphisms, short insertion/deletion and the manually
539 identified copy number variants for further analysis. Chromosomal aberrations were ignored
540 because breseq appears to have a high false positive rate (average of 27 "junction" calls per
541 population across all timepoints). Variants were filtered in three successive steps. (1) Variants
542 not identified in multiple consecutive time points were removed. (2) Variants supported by less
543 than 10 reads across all timepoints in a given population were removed. (3) Since we observed
544 fixation events in every population and since there should be no DNA exchange, all truly
545 segregating variants present in a population at generation 100 must either be fixed or lost in
546 generations 900 and 1000. Thus, we removed variants that failed to do so.

547 Variants that were present at an average frequency $\geq$ 95% at generation 100 across at least 18
548 populations were denoted as ancestral mutations that differentiate the founder from the reference
549 genome (n = 10). Variants that were not ancestral but present at $\geq$ 95% on average across all
550 populations derived from one founder were denoted as founder mutations (n = 11). These
551 mutations were likely introduced as a byproduct of the strain engineering process. Multiallelic
552 variants (two or more derived alleles present in a single population at the same site) were also
553 removed as likely mapping artifacts. Finally, variants that were present at generation 100 in 11+
554 populations (of 36 total sequenced populations) are either mapping artifacts or pre-existing
555 variants and were not considered further (n = 169, including the 10 ancestral mutations identified
556 earlier).

bioRxiv preprint doi: https://doi.org/10.1101/850644; this version posted November 24, 2019. The copyright holder for this preprint (which was not certified by peer review) is the author/funder, who has granted bioRxiv a license to display the preprint in perpetuity. It is made available under aCC-BY-NC 4.0 International license.

557 ## Identification of adaptive mutations

558 The putatively adaptive mutations were identified as follows. We first identified mutations that
559 reached at least 10% frequency, were present in at least two consecutive time points and whose
560 frequency changed by at least 20% throughout the evolution. We then merged together such
561 mutations within 10 bp of each other as likely being derived from a single event. This resulted in
562 a set of candidate adaptive mutations. To identify likely adaptive mutations in this candidate set,
563 we considered only mutations in "multihit" genes, i.e., genes with 2 or more candidate adaptive
564 mutations.

565 ## Identification of modules in the genome

566 The 215 genes annotated as being associated with translation were identified using the Gene
567 Ontology database at http://geneontology.org/ by searching for all *E. coli* K12 genes that were
568 identified in a search for "translation OR ribosom". Similarly, the 45 genes associated with
569 cytokinesis were identified using a search for "cytokinesis".

570 # Statistical analyses

571 The expected number of mutations in multihit genes was calculated via multinomial sampling.
572 Mutations were randomly redistributed across all genes in the *E. coli* genome controlling for
573 variation in gene length. The average of 10,000 such randomizations was used to calculate an
574 empirical FDR. A similar procedure was used to estimate the probability of observed as many or
575 more TM-specific mutations by chance as we actually observed in this study.

576 To test whether mutations in the 7 TM-specific multi-hit loci were distributed uniformly across
577 the six founders we first estimated the entropy of the distribution of mutations across founders
578 for each gene. Mutations in that gene were then randomly redistributed across six founders
579 10,000 times, weighted by the total number of TM-specific mutations observed in each founder.
580 An empirical *P*-value was calculated as the fraction trials with smaller than observed entropy
581 value. These *P*-values were then corrected for multiple testing across the 7 TM-specific loci
582 using the Benjamini-Hochberg procedure. We used the same procedure to test for significant
583 deviations in the distributions of generic mutations across founders.

584

bioRxiv preprint doi: https://doi.org/10.1101/850644; this version posted November 24, 2019. The copyright holder for this preprint (which was not certified by peer review) is the author/funder, who has granted bioRxiv a license to display the preprint in perpetuity. It is made available under aCC-BY-NC 4.0 International license.

585 # Acknowledgements

586 We thank members of the Kryazhimskiy and Kaçar groups, Joanna Masel, Ryan Gutenkunst,
587 Suparna Sanyal, Grant Kinsler, Justin Meyer, and Lin Chao for input and feedback. We thank
588 Alex Pleşa, Divjot Kaur, Emily Peñaherrera, Kevin Longoria and Lesly Villarejo for laboratory
589 assistance. We thank Huanyu Kuo for the analysis of growth-curve data. We thank Eva
590 Garmendia for providing the recombineering plasmids and Georg Rieckh for providing the
591 resistance marker plasmids. We thank Benjamin Good for help with his genome sequencing data
592 analysis pipeline. We thank Kristen Jepsen and the UCSD Institute for Genomic Medicine for
593 sequencing services and the San Diego Supercomputing Center for providing the computational
594 environment. BK acknowledges the support by the John Templeton Foundation (#58562 and
595 #61239); the NASA Exobiology and Evolutionary Biology Program (#H006201406) and the
596 NASA Astrobiology Institute (#NNA17BB05A). SK acknowledges the support by BWF Career
597 Award at the Scientific Interface (#1010719.01), the Alfred P. Sloan Foundation (#FG-2017-
598 9227) and the Hellman Foundation.

bioRxiv preprint doi: https://doi.org/10.1101/850644; this version posted November 24, 2019. The copyright holder for this preprint (which was not certified by peer review) is the author/funder, who has granted bioRxiv a license to display the preprint in perpetuity. It is made available under aCC-BY-NC 4.0 International license.

599 # References

600 1. Simon HA. The Architecture of Complexity. Proc Am Phil Soc. 1962;106: 467–482.

601 2. Valentine JW, May CL. Hierarchies in Biology and Paleontology. Paleobiology. 1996;22: 23–33.

602 3. McShea DW. The hierarchical structure of organisms: a scale and documentation of a trend in the
603 maximum. Paleobiology. 2001;27: 405–423.

604 4. Ravasz E, Somera AL, Mongru DA, Oltvai ZN, Barabási AL. Hierarchical organization of
605 modularity in metabolic networks. Science. 2002;297: 1551–1555.

606 5. Mengistu H, Huizinga J, Mouret J-B, Clune J. The Evolutionary Origins of Hierarchy. PLoS Comput
607 Biol. 2016;12: e1004829.

608 6. Hartwell LH, Hopfield JJ, Leibler S, Murray AW. From molecular to modular cell biology. Nature.
609 1999;402: C47–52.

610 7. Wagner GP, Pavlicev M, Cheverud JM. The road to modularity. Nat Rev Genet. 2007;8: 921–931.

611 8. Woese C. Molecular mechanics of translation: a reciprocating ratchet mechanism. Nature. 1970;226:
612 817–820.

613 9. Frank J. The ribosome--a macromolecular machine par excellence. Chem Biol. 2000;7: R133–41.

614 10. Fisher R. The genetical theory of natural selection. Oxford University Press; 1930.

615 11. Kacser H, Burns JA. The molecular basis of dominance. Genetics. 1981;97: 639–666.

616 12. Hartl DL, Taubes CH. Towards a theory of evolutionary adaptation. Genetica. 1998;102-103: 525–
617 533.

618 13. Orr HA. The population genetics of adaptation: the distribution of factors fixed during adaptive
619 evolution. Evolution. 1998;52: 935–949.

620 14. Welch JJ, Waxman D. Modularity and the cost of complexity. Evolution. 2003;57: 1723–1734.

621 15. Orr HA. The genetic theory of adaptation: a brief history. Nat Rev Genet. 2005;6: 119–127.

622 16. Orr HA. The distribution of fitness effects among beneficial mutations in Fisher's geometric model
623 of adaptation. J Theor Biol. 2006;238: 279–285.

624 17. Waxman D. Fisher's geometrical model of evolutionary adaptation—Beyond spherical geometry. J
625 Theor Biol. 2006;241: 887–895.

626 18. Martin G, Lenormand T. A general multivariate extension of Fisher's geometrical model and the
627 distribution of mutation fitness effects across species. Evolution. 2006;60: 893–907.

628 19. Martin G, Lenormand T. The distribution of beneficial and fixed mutation fitness effects close to an
629 optimum. Genetics. 2008;179: 907–916.

630 20. Gordo I, Campos PRA. Evolution of clonal populations approaching a fitness peak. Biol Lett.

bioRxiv preprint doi: https://doi.org/10.1101/850644; this version posted November 24, 2019. The copyright holder for this preprint (which was not certified by peer review) is the author/funder, who has granted bioRxiv a license to display the preprint in perpetuity. It is made available under aCC-BY-NC 4.0 International license.

631 2013;9: 20120239.

632 21. Tenaillon O. The Utility of Fisher's Geometric Model in Evolutionary Genetics. Annu Rev Ecol
633 Evol Syst. 2014;45: 179–201.

634 22. Hartl DL, Dykhuizen DE, Dean AM. Limits of adaptation: the evolution of selective neutrality.
635 Genetics. 1985;111: 655–674.

636 23. Lynch M. Evolutionary layering and the limits to cellular perfection. Proc Natl Acad Sci U S A.
637 2012. Available: https://www.pnas.org/content/109/46/18851.short

638 24. Nourmohammad A, Schiffels S, Lässig M. Evolution of molecular phenotypes under stabilizing
639 selection. J Stat Mech: Theory Exp. 2013;2013: P01012.

640 25. Barton NH. Linkage and the limits to natural selection. Genetics. 1995;140: 821–841.

641 26. Gerrish PJ, Lenski RE. The fate of competing beneficial mutations in an asexual population.
642 Genetica. 1998;102-103: 127–144.

643 27. Desai MM, Fisher DS. Beneficial mutation–selection balance and the effect of linkage on positive
644 selection. Genetics. 2007;176: 1759–1798.

645 28. Neher RA, Shraiman BI. Competition between recombination and epistasis can cause a transition
646 from allele to genotype selection. Proc Natl Acad Sci U S A. 2009;106: 6866–6871.

647 29. Good BH, Rouzine IM, Balick DJ, Hallatschek O, Desai MM. Distribution of fixed beneficial
648 mutations and the rate of adaptation in asexual populations. Proc Natl Acad Sci U S A. 2012;109:
649 4950–4955.

650 30. Schiffels S, Szöllosi GJ, Mustonen V, Lässig M. Emergent neutrality in adaptive asexual evolution.
651 Genetics. 2011;189: 1361–1375.

652 31. Lang GI, Botstein D, Desai MM. Genetic variation and the fate of beneficial mutations in asexual
653 populations. Genetics. 2011;188: 647–661.

654 32. Lang GI, Rice DP, Hickman MJ, Sodergren E, Weinstock GM, Botstein D, et al. Pervasive genetic
655 hitchhiking and clonal interference in forty evolving yeast populations. Nature. 2013;500: 571–574.

656 33. Kao KC, Sherlock G. Molecular characterization of clonal interference during adaptive evolution in
657 asexual populations of Saccharomyces cerevisiae. Nat Genet. 2008;40: 1499–1504.

658 34. Kvitek DJ, Sherlock G. Whole genome, whole population sequencing reveals that loss of signaling
659 networks is the major adaptive strategy in a constant environment. PLoS Genet. 2013;9: e1003972.

660 35. Herron MD, Doebeli M. Parallel evolutionary dynamics of adaptive diversification in Escherichia
661 coli. PLoS Biol. 2013;11: e1001490.

662 36. Tenaillon O, Rodríguez-Verdugo A, Gaut RL, McDonald P, Bennett AF, Long AD, et al. The
663 molecular diversity of adaptive convergence. Science. 2012;335: 457–461.

664 37. Kryazhimskiy S, Rice DP, Jerison ER, Desai MM. Global epistasis makes adaptation predictable
665 despite sequence-level stochasticity. Science. 2014;344: 1519–1522.

bioRxiv preprint doi: https://doi.org/10.1101/850644; this version posted November 24, 2019. The copyright holder for this preprint (which was not certified by peer review) is the author/funder, who has granted bioRxiv a license to display the preprint in perpetuity. It is made available under aCC-BY-NC 4.0 International license.

666 38. Szamecz B, Boross G, Kalapis D, Kovács K, Fekete G, Farkas Z, et al. The genomic landscape of
667 compensatory evolution. PLoS Biol. 2014;12: e1001935.

668 39. Jerison ER, Kryazhimskiy S, Mitchell JK, Bloom JS, Kruglyak L, Desai MM. Genetic variation in
669 adaptability and pleiotropy in budding yeast. Elife. 2017;6.

670 40. Good BH, McDonald MJ, Barrick JE, Lenski RE, Desai MM. The dynamics of molecular evolution
671 over 60,000 generations. Nature. 2017;551: 45–50.

672 41. Rojas Echenique JI, Kryazhimskiy S, Nguyen Ba AN, Desai MM. Modular epistasis and the
673 compensatory evolution of gene deletion mutants. PLoS Genet. 2019;15: e1007958.

674 42. Gresham D, Desai MM, Tucker CM, Jenq HT, Pai DA, Ward A, et al. The repertoire and dynamics
675 of evolutionary adaptations to controlled nutrient-limited environments in yeast. PLoS Genet.
676 2008;4: e1000303.

677 43. Hong J, Gresham D. Molecular specificity, convergence and constraint shape adaptive evolution in
678 nutrient-poor environments. PLoS Genet. 2014;10: e1004041.

679 44. Payen C, Di Rienzi SC, Ong GT, Pogachar JL, Sanchez JC, Sunshine AB, et al. The dynamics of
680 diverse segmental amplifications in populations of Saccharomyces cerevisiae adapting to strong
681 selection. G3 . 2014;4: 399–409.

682 45. Couñago R, Chen S, Shamoo Y. In vivo molecular evolution reveals biophysical origins of
683 organismal fitness. Mol Cell. 2006;22: 441–449.

684 46. Chou H-H, Delaney NF, Draghi JA, Marx CJ. Mapping the fitness landscape of gene expression
685 uncovers the cause of antagonism and sign epistasis between adaptive mutations. PLoS Genet.
686 2014;10: e1004149.

687 47. Michener JK, Neves AAC, Vuilleumier S, Bringel F, Marx CJ. Effective use of a horizontally-
688 transferred pathway for dichloromethane catabolism requires post--transfer refinement. Elife.
689 2014;3: e04279.

690 48. Venkataram S, Dunn B, Li Y, Agarwala A, Chang J, Ebel ER, et al. Development of a
691 Comprehensive Genotype-to-Fitness Map of Adaptation-Driving Mutations in Yeast. Cell.
692 2016;166: 1585–1596.e22.

693 49. Rodrigues JV, Shakhnovich EI. Adaptation to mutational inactivation of an essential gene converges
694 to an accessible suboptimal fitness peak. Elife. 2019;8. doi:10.7554/eLife.50509

695 50. Laan L, Koschwanez JH, Murray AW. Evolutionary adaptation after crippling cell polarization
696 follows reproducible trajectories. Elife. 2015;4. doi:10.7554/eLife.09638

697 51. Ramakrishnan V. Ribosome structure and the mechanism of translation. Cell. 2002;108: 557–572.

698 52. Williamson JR. The ribosome at atomic resolution. Cell. 2009;139: 1041–1043.

699 53. Melnikov S, Ben-Shem A, Garreau de Loubresse N, Jenner L, Yusupova G, Yusupov M. One core,
700 two shells: bacterial and eukaryotic ribosomes. Nat Struct Mol Biol. 2012;19: 560–567.

701 54. Savir Y, Tlusty T. The ribosome as an optimal decoder: a lesson in molecular recognition. Cell.
702 2013;153: 471–479.

bioRxiv preprint doi: https://doi.org/10.1101/850644; this version posted November 24, 2019. The copyright holder for this preprint (which was not certified by peer review) is the author/funder, who has granted bioRxiv a license to display the preprint in perpetuity. It is made available under aCC-BY-NC 4.0 International license.

703 55. Kaçar B, Garmendia E, Tuncbag N, Andersson DI, Hughes D. Functional Constraints on Replacing
704 an Essential Gene with Its Ancient and Modern Homologs. MBio. 2017;8. doi:10.1128/mBio.01276-
705 17

706 56. Miller DL, Weissbach H. Factors involved in the transfer of aminoacyl-tRNA to the ribosome. In:
707 Petska S, Weissbach H, editors. Molecular mechanisms of protein biosynthesis. Academic Press,
708 London; 1977. pp. 323–373.

709 57. Nilsson J, Nissen P. Elongation factors on the ribosome. Curr Opin Struct Biol. 2005;15: 349–354.

710 58. Scott M, Gunderson CW, Mateescu EM, Zhang Z, Hwa T. Interdependence of Cell Growth and
711 Gene Expression: Origins and Consequences. Science. 2010;330: 1099–1102.

712 59. Tubulekas I, Hughes D. Suppression of rpsL phenotypes by tuf mutations reveals a unique
713 relationship between translation elongation and growth rate. Mol Microbiol. 1993;7: 275–284.

714 60. Schnell R, Abdulkarim F, Kálmán M, Isaksson LA. Functional EF-Tu with large C-terminal
715 extensions in an E. coli strain with a precise deletion of both chromosomal tuf genes. FEBS Lett.
716 2003;538: 139–144.

717 61. Lenski RE, Mongold JA, Sniegowski PD, Travisano M, Vasi F, Gerrish PJ, et al. Evolution of
718 competitive fitness in experimental populations of E. coli: what makes one genotype a better
719 competitor than another? Antonie Van Leeuwenhoek. 1998;73: 35–47.

720 62. Li Y, Venkataram S, Agarwala A, Dunn B, Petrov DA, Sherlock G, et al. Hidden Complexity of
721 Yeast Adaptation under Simple Evolutionary Conditions. Curr Biol. 2018;28: 515–525.e6.

722 63. Manhart M, Adkar BV, Shakhnovich EI. Trade-offs between microbial growth phases lead to
723 frequency-dependent and non-transitive selection. Proc Biol Sci. 2018;285.

724 64. Vasi F, Travisano M, Lenski RE. Long-Term Experimental Evolution in Escherichia coli. II.
725 Changes in Life-History Traits During Adaptation to a Seasonal Environment. Am Nat. 1994;144:
726 432–456.

727 65. Utnes ALG, Sørum V, Hülter N, Primicerio R, Hegstad J, Kloos J, et al. Growth phase-specific
728 evolutionary benefits of natural transformation in Acinetobacter baylyi. ISME J. 2015;9: 2221–2231.

729 66. Khan AI, Dinh DM, Schneider D, Lenski RE, Cooper TF. Negative epistasis between beneficial
730 mutations in an evolving bacterial population. Science. 2011;332: 1193–1196.

731 67. Wünsche A, Dinh DM, Satterwhite RS, Arenas CD, Stoebel DM, Cooper TF. Diminishing-returns
732 epistasis decreases adaptability along an evolutionary trajectory. Nat Ecol Evol. 2017;1: 61.

733 68. Wiser MJ, Ribeck N, Lenski RE. Long-term dynamics of adaptation in asexual populations. Science.
734 2013;342: 1364–1367.

735 69. Schoustra SE, Bataillon T, Gifford DR, Kassen R. The properties of adaptive walks in evolving
736 populations of fungus. PLoS Biol. 2009;7: e1000250.

737 70. Couce A, Tenaillon OA. The rule of declining adaptability in microbial evolution experiments. Front
738 Genet. 2015;6: 99.

739 71. Tenaillon O, Silander OK, Uzan J-P, Chao L. Quantifying organismal complexity using a population

bioRxiv preprint doi: https://doi.org/10.1101/850644; this version posted November 24, 2019. The copyright holder for this preprint (which was not certified by peer review) is the author/funder, who has granted bioRxiv a license to display the preprint in perpetuity. It is made available under aCC-BY-NC 4.0 International license.

740 genetic approach. PLoS One. 2007;2: e217.

741 72. Asai T, Zaporojets D, Squires C, Squires CL. An Escherichia coli strain with all chromosomal rRNA
742 operons inactivated: complete exchange of rRNA genes between bacteria. Proc. Natl. Acad. Sci. U.
743 S. A. 1999. pp. 1971–1976.

744 73. Dutheil JY, Jossinet F, Westhof E. Base pairing constraints drive structural epistasis in ribosomal
745 RNA sequences. Mol Biol Evol. 2010;27: 1868–1876.

746 74. Barreto FS, Burton RS. Evidence for compensatory evolution of ribosomal proteins in response to
747 rapid divergence of mitochondrial rRNA. Mol Biol Evol. 2013;30: 310–314.

748 75. Sloan DB, Triant DA, Wu M, Taylor DR. Cytonuclear interactions and relaxed selection accelerate
749 sequence evolution in organelle ribosomes. Mol Biol Evol. 2014;31: 673–682.

750 76. Shah P, McCandlish DM, Plotkin JB. Contingency and entrenchment in protein evolution under
751 purifying selection. Proc Natl Acad Sci U S A. 2015;112: E3226–35.

752 77. Starr TN, Flynn JM, Mishra P, Bolon DNA, Thornton JW. Pervasive contingency and entrenchment
753 in a billion years of Hsp90 evolution. Proc Natl Acad Sci U S A. 2018;115: 4453–4458.

754 78. Blount ZD, Lenski RE, Losos JB. Contingency and determinism in evolution: Replaying life's tape.
755 Science. 2018;362.

756 79. Orr HA. The distribution of fitness effects among beneficial mutations. Genetics. 2003;163: 1519–
757 1526.

758 80. Levy SF, Blundell JR, Venkataram S, Petrov DA, Fisher DS, Sherlock G. Quantitative evolutionary
759 dynamics using high-resolution lineage tracking. Nature. 2015;519: 181.

760 81. Chou H-H, Chiu H-C, Delaney NF, Segrè D, Marx CJ. Diminishing returns epistasis among
761 beneficial mutations decelerates adaptation. Science. 2011;332: 1190–1192.

762 82. MacLean RC, Perron GG, Gardner A. Diminishing returns from beneficial mutations and pervasive
763 epistasis shape the fitness landscape for rifampicin resistance in Pseudomonas aeruginosa. Genetics.
764 2010;186: 1345–1354.

765 83. Wei X, Zhang J. Patterns and mechanisms of diminishing returns from beneficial mutations. Mol
766 Biol Evol. 2019.

767 84. Lind PA, Tobin C, Berg OG, Kurland CG, Andersson DI. Compensatory gene amplification restores
768 fitness after inter-species gene replacements. Mol Microbiol. 2010;75: 1078–1089.

769 85. Kacar B, Ge X, Sanyal S, Gaucher EA. Experimental Evolution of Escherichia coli Harboring an
770 Ancient Translation Protein. J Mol Evol. 2017;84: 69–84.

771 86. Wagner A. Neutralism and selectionism: a network-based reconciliation. Nat Rev Genet. 2008;9:
772 965–974.

773 87. Schaper S, Johnston IG, Louis AA. Epistasis can lead to fragmented neutral spaces and contingency
774 in evolution. Proc Biol Sci. 2012;279: 1777–1783.

775 88. Newman MEJ, Engelhardt R. Effects of selective neutrality on the evolution of molecular species.

bioRxiv preprint doi: https://doi.org/10.1101/850644; this version posted November 24, 2019. The copyright holder for this preprint (which was not certified by peer review) is the author/funder, who has granted bioRxiv a license to display the preprint in perpetuity. It is made available under aCC-BY-NC 4.0 International license.

776 Proc Roy Soc B: Biological Sciences. 1998;265: 1333–1338.

777 89. Zaslaver A, Mayo AE, Rosenberg R, Bashkin P, Sberro H, Tsalyuk M, et al. Just-in-time
778 transcription program in metabolic pathways. Nat Genet. 2004;36: 486–491.

779 90. Chung CT, Niemela SL, Miller RH. One-step preparation of competent Escherichia coli:
780 transformation and storage of bacterial cells in the same solution. Proc Natl Acad Sci U S A.
781 1989;86: 2172–2175.

782 91. Geissmann Q. OpenCFU, a new free and open-source software to count cell colonies and other
783 circular objects. PLoS One. 2013;8: e54072.

784 92. Baym M, Kryazhimskiy S, Lieberman TD, Chung H, Desai MM, Kishony R. Inexpensive
785 multiplexed library preparation for megabase-sized genomes. PLoS One. 2015;10: e0128036.

786 93. Wang K, Li M, Hakonarson H. ANNOVAR: functional annotation of genetic variants from high-
787 throughput sequencing data. Nucleic Acids Res. 2010;38: e164.

788 94. Trapnell C, Roberts A, Goff L, Pertea G, Kim D, Kelley DR, et al. Differential gene and transcript
789 expression analysis of RNA-seq experiments with TopHat and Cufflinks. Nat Protoc. 2012;7: 562–
790 578.

791 95. Li H, Handsaker B, Wysoker A, Fennell T, Ruan J, Homer N, et al. The Sequence Alignment/Map
792 format and SAMtools. Bioinformatics. 2009;25: 2078–2079.

793